Research Article

Hao Li*, Zhaogang Yu, Kun Liu, Zhen Tao, and Jiangtao Zhang

Damage accumulation and failure mechanism of glass/epoxy composite laminates subjected to repeated low velocity impacts

https://doi.org/10.1515/epoly-2023-0146
received September 18, 2023; accepted November 25, 2023

Abstract: In this work, the damage accumulation and failure mechanism of glass fiber-reinforced epoxy composite laminates under repeated low velocity impacts were studied considering the influence of stacking sequence. The typical sandwich-like $[0°_2/90°_2]_s$, angle-ply $[\pm45°]_{2s}$ and quasi-isotropic $[0°/-45°/45°/90°]_s$ laminates were tested at 20 J impact energy. The impact responses including contact force–time/central displacement and energy–time curves were recorded. The tendencies of the peak contact force, maximum displacement, bending stiffness, and energy dissipation with the increase in impact number were analyzed. Damage induced in the laminates was further evaluated. The results show that the impact resistance of the sandwich-like laminate is the weakest with the lowest peak load and the highest energy dissipation. The impact resistance of the quasi-isotropic laminate is better relative to the angle-ply laminate before the occurrence of fiber breakage, whereas the damage tolerance of the angle-ply laminate is higher with relatively slower damage accumulation at subsequent impacts.

Keywords: composite laminates, repeated low velocity impact, stacking sequence, damage accumulation, impact resistance

*** Corresponding author: Hao Li,** Jiangxi Key Laboratory of Disaster Prevention-Mitigation and Emergency Management, East China Jiaotong University, Nanchang 330013, China; Institute of Disaster Prevention and Mitigation Engineering and Protection Engineering, School of Civil Engineering and Architecture, East China Jiaotong University, Nanchang 330013, China, e-mail: lihao3093@163.com
Zhaogang Yu, Kun Liu, Zhen Tao, Jiangtao Zhang: Jiangxi Key Laboratory of Disaster Prevention-Mitigation and Emergency Management, East China Jiaotong University, Nanchang 330013, China; Institute of Disaster Prevention and Mitigation Engineering and Protection Engineering, School of Civil Engineering and Architecture, East China Jiaotong University, Nanchang 330013, China

1 Introduction

Fiber-reinforced composites are the most prominent materials nowadays attributed to their lightweight, significant strength, high stiffness, and convenient for industrial manufacture. They have been widely employed in aerospace, automotive, marine, and other fields (1–4). However, composites are sensitive to transverse loading such as low velocity impact load owing to their out-of-plane low load bearing capacity. In past decades, numerous investigations have been carried out on the low velocity impact responses and damage development of composite laminates (5–9). Typical damage modes such as matrix cracking and fiber breaking induced in intralaminar, and delamination caused at interlaminar are revealed during single low velocity impact process, which is the well-known barely visible impact damage that weakens the mechanical performance of the composite laminates. In most realistic cases, composite laminates are more likely to encounter repeated impacts than a single localized impact during the process of production, daily maintenance, and service life (10,11). Although only small damage is generated in each single impact, these defects can easily accumulate under repeated impacts, leading to severe damage and cause major mechanical properties degradation (12). Therefore, the necessity to investigate fiber-reinforced composites subjected to repeated impacts becomes apparent.

Abundance of research works on the repeated impact dynamic behaviors and damage mechanism of polymer composites have been carried out over the past decades. Many scholars have focused on the effects of impact angle (13) and energy (14,15), impactor shapes (16) and diameter (17), and external environmental conditions such as thermal aging (18) and low temperature (19) on the dynamic responses and damage accumulation of polymer composites subjected to repeated low velocity impacts. Dogan (16) investigated the influences of impactor shapes on the repeated impact responses of the thermoplastic and thermoset matrix-based composite panels. Compared with the shape of hemisphere,

the repeated impact number achieving penetration decreased dramatically in conical impact cases. The influence of impactor diameter on the repeated low velocity impact response and damage accumulation mechanism of composite laminates was investigated by Liao et al. (17). A new damage evaluation index DI-B was proposed based on bending stiffness reduction rate and normalized maximum displacement, which could characterize the damage accumulation of fiber-reinforced composite laminates and distinguish the appearance of perforation well. The repeated low velocity impact testing was also performed to reveal the impact mechanical responses of repaired polymer composites (20,21), fiber metal laminates (22,23), and sandwich structures (24,25). Both experimental and numerical methods were adopted by Sun et al. (21) to determine the damage evolution and energy dissipation of patch-repaired composite laminates under repeated impacts. Their work indicated that the delamination damage closely reflected the damage accumulation degree of patch-repaired composites subjected to repeated impacts. In addition, many investigations have been conducted on the repeated impact responses and damage mechanism of the composite laminates with different material types (26,27), ply stacking sequences (28,29), and thicknesses (30,31). The repeated low velocity impact dynamic responses of the hybrid plain-woven graphite and glass fiber-reinforced composite laminates with two sandwich lay-up configurations (28) and the balanced carbon fiber-reinforced laminates (symmetric, asymmetric, and antisymmetric) (29) have been explored. However, there are few reports on the influence of stacking sequence on the impact behavior of glass fiber-reinforced composite laminates subjected to repeated low velocity impacts. The stacking pattern is crucial for the impact resistance and damage accumulation of composite laminates under successive impacts, needing more attention and exploration.

In this study, the repeated low velocity impact dynamic responses and damage accumulation of unidirectional glass fiber-reinforced composite laminates with three representative lay-up structures were studied. First, the repeated impact testing was conducted until the occurrence of the perforation. The impact mechanical behaviors such as the impact contact force, central displacement and energy vs time curves were recorded. The variations in the mechanical responses including peak impact force, maximum central displacement, bending stiffness, and energy dissipation were analyzed. Then, the external and internal damage was identified using the nondestructive and destructive methods containing visual inspection, stereo microscope, ultrasonic C-scan technique, and scanning electron microscope (SEM). The impact resistance and damage evolution of the three stacking configurations were determined. Finally, the damage accumulation of the studied composite laminates was evaluated employing two typical damage variables, and the influence of stacking sequences on the damage accumulation was analyzed.

2 Experimental procedure

2.1 Specimen preparation

In this study, the unidirectional glass fiber and vinyl ester resin were employed as the reinforced fiber and matrix material for the composite laminates, respectively. Added with the hardening agent of methyl ethyl ketone peroxide and the accelerating agent of dimethylaniline, the resin can be well cured at room temperature. The weight ratio of the resin, hardening agent, and accelerating agent was specified as 100:1:0.2. The surface density of the unidirectional glass fiber cloth with one layer thickness of 0.25 mm was 450 g·m^{-2}. And the tensile mechanical properties of the glass fiber cloth were 72 GPa in modulus and 1.57 GPa in strength, respectively. All the experimental materials mentioned above were purchased from Tongxiang Mengtai Reinforced Composite Material Company (Tongxiang, China).

The composite laminates were manufactured by the VARI technology which was usually applied to the thermosetting composites. The schematic diagram of the VARI process is displayed in Figure 1. The preparation of the original composite plates was completed on the smooth and clean glass plate placed on a table. One layer release cloth, glass fiber clothes, one layer release cloth, and the diversion net were arranged on the work bench from the bottom to top. The preparation laminates can be easily separated from the work bench with the help of release clothes on each side. Guided by the diversion net, the fiber clothes can be saturated with resin uniformly. The whole system was covered by a vacuum bag and was in vacuum environment after the work of vacuum pump. After the injection of resin, the system was cured for 24 h at the vacuum level of 650 mbar. The original laminates with three stacking sequences of $[0°_2/90°_2]_s$, $[\pm45°]_{2s}$, and $[0°/-45°/45°/90°]_s$ were fabricated. The specimens with the dimension of 150 mm × 100 mm × 2.8 mm were cut from the original laminates using a diamond saw blade cutting machine.

2.2 Repeated low velocity impact testing

According to the ASTM D7136 standard, repeated low velocity impact testing was performed using the Instron

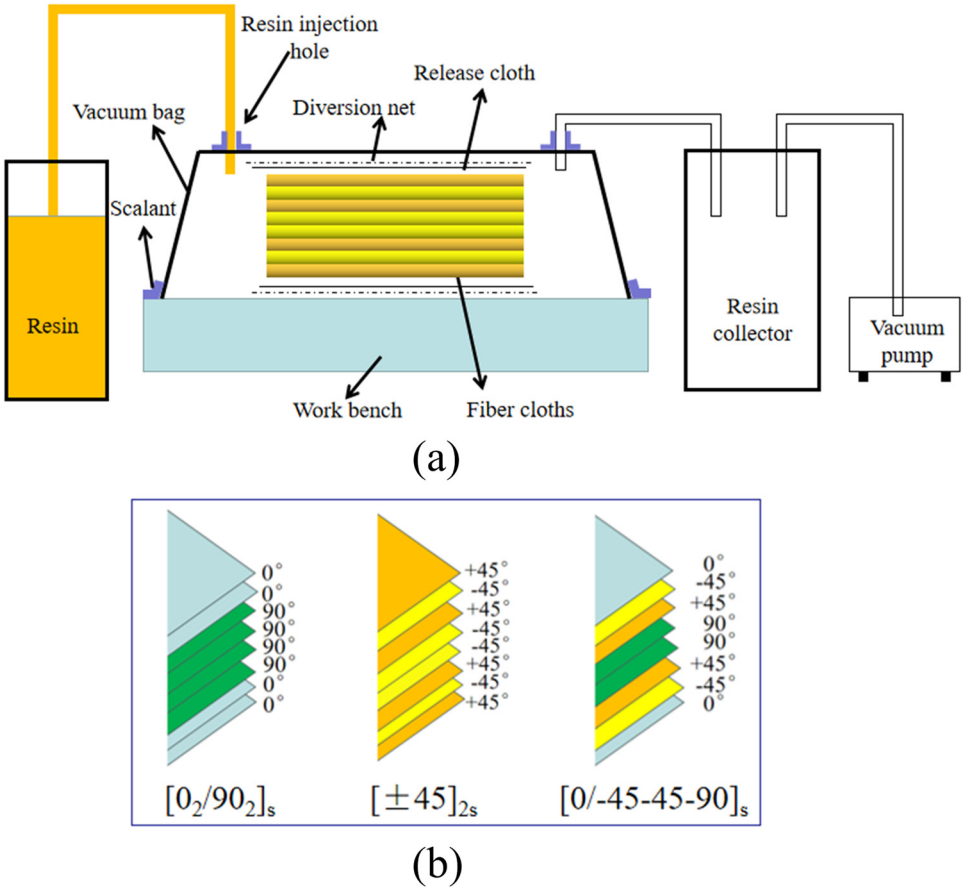

Figure 1: Specimen preparation: (a) vacuum-assisted resin injection (VARI) process and (b) the studied stacking sequences.

Dynatup CEAST 9340 machine at room temperature, as presented in Figure 2. The test platform was mainly composed of the specimen fixture, a drop hammer device, and a data acquisition system. During the impact event, composite specimens were firmly fastened between two steel plates with 76 mm diameter hole at the center. Controlled by the control platform, the impactor fell from the specified impact height. Then, the impactor struck the center of the specimen and bounced up after the process of contact. Finally, the impactor was caught by the anti-secondary impact device avoiding the second impact. Above the projectile head, a piezo-electric load cell as the dynamic force sensor was used to measure the impact contact force. The contact force data were collected by the data acquisition system in real time, which was employed to calculate the impact kinetic energy of the impactor combining the initial impact velocity at the moment of impact occurrence. The hemispherical impactor with 16 mm diameter and 8 kg weight was raised to the initial given height to implement low velocity impacts. The impact energy level was set as 20 J, corresponding to the initial impact velocity of 2.236 $m \cdot s^{-1}$ in this work. The repeated low velocity impact tests were realized by raising the impactor to the initial given height after previous impact. To guarantee the reliability of the testing, five specimens were struck for each stacking sequence. To evaluate the induced damage, the external damage morphology on both surfaces was observed by visual inspection, the extent of the internal damage was detected applying the stereo microscope and ultrasonic C-scan technique, and the micro-damage morphology of the central damage region was determined by means of the SEM.

3 Results and discussion

3.1 Repeated impact dynamic mechanical responses

The impact contact force–time/displacement curves of the specimens with the stacking sequences of $[0°_2/90°_2]_s$, $[\pm45°]_{2s}$, and $[0°/-45°/45°/90°]_s$ under repeated low velocity impacts are plotted in Figure 3. The specimens experience similar

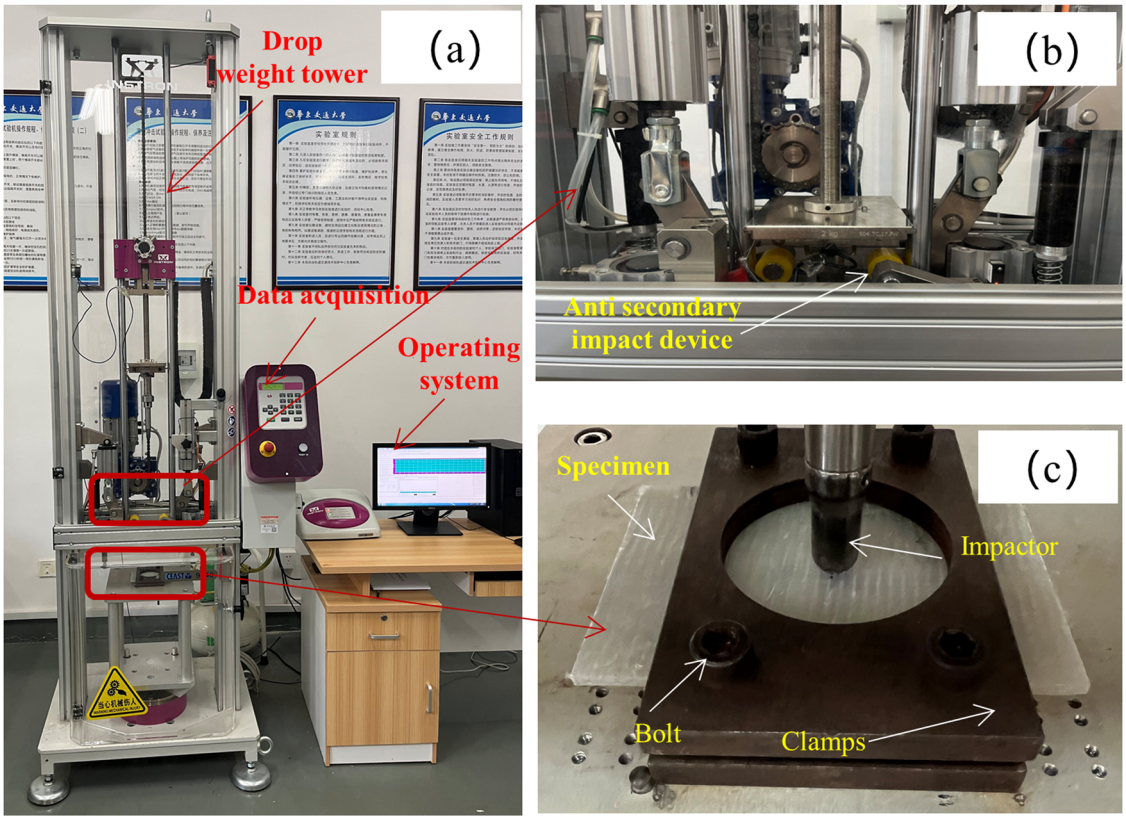

Figure 2: Setup of the low velocity impact testing: (a) drop weight impact testing machine, (b) anti-secondary impact device, and (c) fixed specimen.

impact response trend regardless of the stacking sequence during the impact test, starting with the typical rebounding curve at low impact number, followed by the penetration feature with the impactor gradually embedding into the specimen, until the occurrence of the perforation representing the failure of the specimen. For each lay-up configuration, the impact contact peak force first increases and then decreases with the increase in impact number, and the maximum central displacement of the specimen increases with the rise in impact number until the perforation.

As shown in Figure 3(a–c), each of the stacking configurations exhibits four typical characteristics of the force–time and force–displacement curves during the repeated impact tests, namely, the initial local fluctuation in the ascending stage of the first impact, a drop of the impact force before reaching the peak force, large drop of the impact force, and almost constant plateau of the impact force. The four typical features of impact responses are closely related to the damage induced in the specimen. With the help of stereo microscope, the transverse damage morphology corresponding the four stages was detected and displayed in Figure 3(d). It is observed that the initial local fluctuation in the rising phase of the first impact is mainly caused by the unstable damage propagation of matrix cracking and the initiation of delamination. The damage mode of matrix cracking is clearly observed through the thickness of the specimens with all stacking sequences. Similar phenomenon also appeared in the works of Sun et al. (21) and Rezasefat et al. (32). It is the first time the impact force has a drop before reaching the peak value at the second impact for the specimens with the stacking sequences of $[\pm 45°]_{2s}$ and $[0°/-45°/45°/90°]_s$, and at the third impact for the specimen with the lay-up sequence of $[0°_2/90°_2]_s$. As indicated in literature (17,33), this impact characteristic can be regarded as the known delamination threshold, describing a distinguishable drop of the impact force in the ascending stage. The distinct delamination presented by the damage morphology in the cross-section of the specimens demonstrates this phenomenon. The contact force has an obvious drop just reaching the peak value at the 5th, 11th, and 7th impact for the specimens with the stacking sequences of $[0°_2/90°_2]_s$, $[\pm 45°]_{2s}$, and $[0°/-45°/45°/90°]_s$, respectively. The sharp force drop can be explained by the appearance of fiber breakage, which can be demonstrated by the transverse damage morphology at the region beneath the impactor acquired by the stereo microscope technique. This is consistent with the phenomenon found in previous research works (28,31). The impact force becomes approximately constant

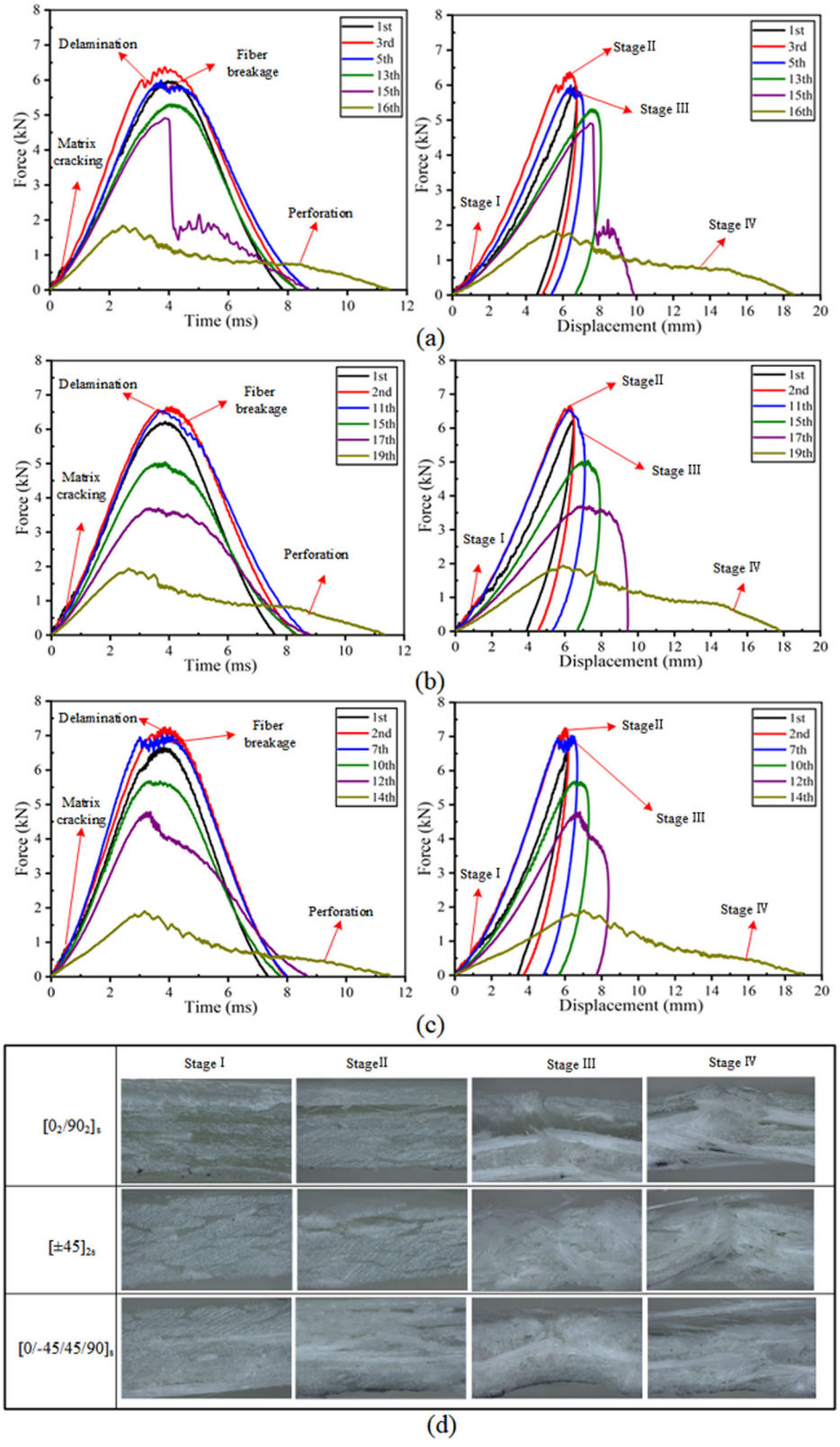

Figure 3: Repeated impact responses (contact force vs time and force–displacement curves) and the corresponding damage morphology detected by stereo microscope: (a) specimens with the lay-up sequence of $[0°_2/90°_2]_S$, (b) specimens with the ply orientation of $[\pm45°]_{2S}$, (c) specimens with the stacking sequence of $[0°/-45°/45°/90°]_S$, and (d) damage morphology at the four stages.

value at the 16th, 19th, and 14th impact for the specimens with the lay-up sequences of $[0°_2/90°_2]_s$, $[\pm45°]_{2s}$, and $[0°/-45°/45°/90°]_s$, respectively. As reported in previous studies (34,35), the appearance of constant force plateau reveals the occurrence of perforation of the specimen. The contact force is produced resulting from the friction between the impactor and the laminate during the insertion process, thus the impact force keeps a roughly stable value. Indeed, large amounts of fiber breakage through the thickness is observed in a cross-section view.

The representative energy–time curves of the three laminated specimens during repeated impact testing are illustrated in Figure 4. During an impact event, the impact energy is partly converted into the elastic energy of the laminate, and the other is absorbed by the laminate through plastic deformation, friction, and various failure processes (36). The elastic energy reserved in the laminate is released to rebound the impactor after the contact between the impactor and laminate. Due to the low strain to failure of the glass fiber and the brittle nature of the epoxy resin matrix, the composite laminates show very little or no plastic deformation. Therefore, the absorbed impact energy is mainly dissipated by the damage induced in the laminates, such as matrix cracking, delamination, and fiber breakage. It can be seen that large part of the impact energy is absorbed by the damage for the impact events including the rebounding stage, while relatively less elastic energy is transformed into the kinetic energy of the impactor in the rebounding stage. The absorbed energy first has a little decrease in initial few impact tests and then increases with the rise in the impact number. Moreover, the absorbed energy has an evident increase at the impact number of the appearance of fiber breakage regardless of the stacking sequence. For the perforation event, the impact energy is completely absorbed by the specimens, i.e., the energy absorption reaches the initial impact kinetic energy of the

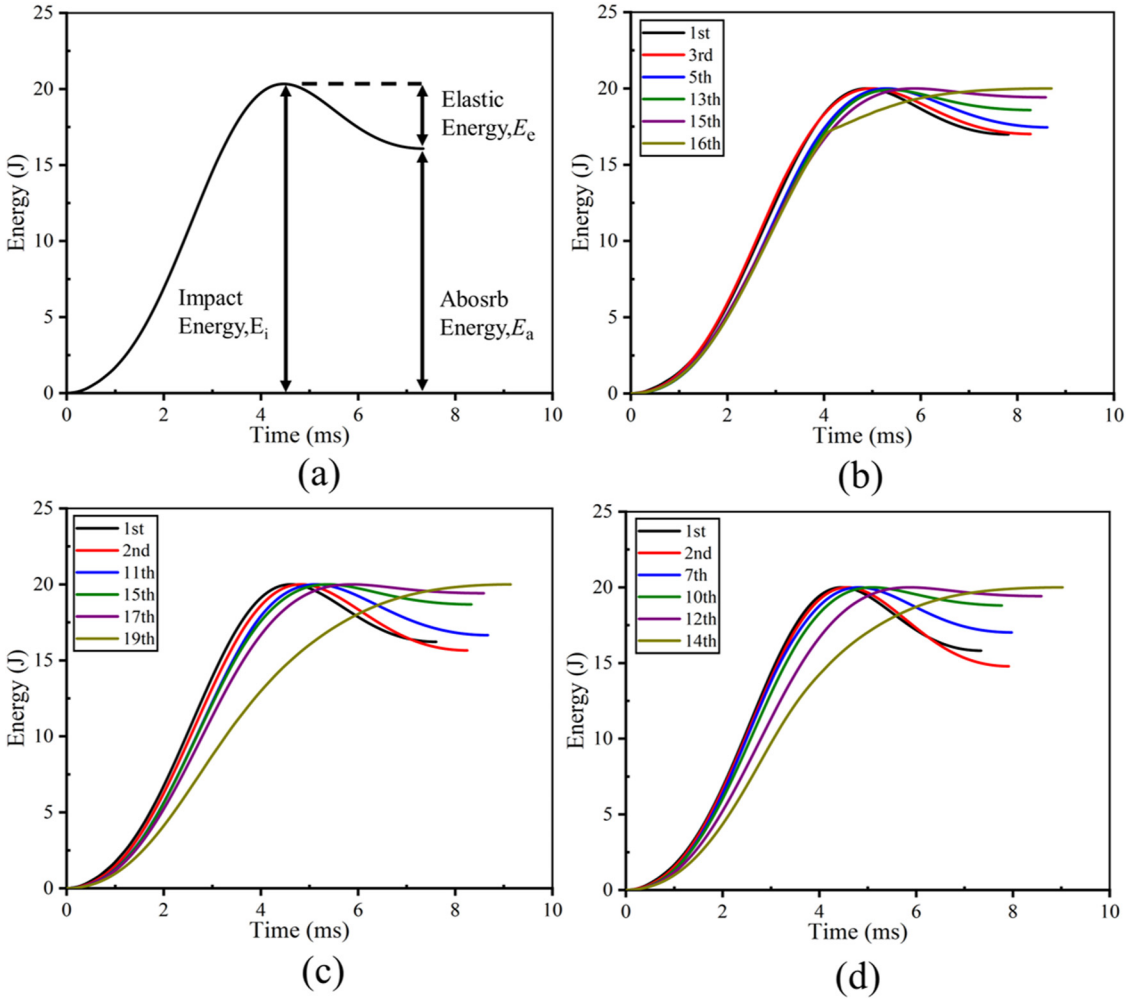

Figure 4: Typical energy vs time curves during repeated impact tests: (a) the schematic diagram of the energy–time curve, (b) the $[0°_2/90°_2]_s$ laminated specimens, (c) the $[\pm45°]_{2s}$ laminated specimens, and (d) the $[0°/-45°/45°/90°]_s$ laminated specimens.

impactor, which is coincided with the indication in the literature (34,37). Hence, the perforation occurs at the 16th, 19th, and 14th impact for the specimens with the stacking sequences of $[0°_2/90°_2]_s$, $[\pm45°]_{2s}$, and $[0°/-45°/45°/90°]_s$, respectively.

3.2 Analysis of the impact mechanical responses

The variations in impact mechanical responses including the peak force, maximum central displacement, absorbed energy, and bending stiffness for the three lay-up specimens under repeated impacts until perforation are plotted in Figure 5. In general, as shown in Figure 5(a), the peak force of the three stacking specimens first increases in the initial few impacts, and then roughly keeps constant plateau, followed by a gradual decrease until the occurrence of perforation. As indicated in works (32,38), the increase in the peak force for the initial few impacts can be attributed to the compaction effect of the laminate. After the first impact, the intact fibers bear the impact loading instead of the damaged matrix beneath the impact location, which results in a local stiffer contact between the impactor and the enhanced phase at the central region for successive few impacts. Thus, the peak force acquires a higher value. With the stable development of matrix cracking and delamination, the impact contact loading is primarily undertaken by the intact fibers, leading to the constant plateau of the peak force. The peak force has a significant drop at the 5th, 11th, and 7th impact for the specimens with the stacking sequences of $[0°_2/90°_2]_s$, $[\pm45°]_{2s}$, and $[0°/-45°/45°/90°]_s$, respectively. This phenomenon results from the appearance of severe damage mode of fiber breakage. Subsequently, the peak force gradually decreases with the intensity of fiber breakage. At the impact of perforation, the peak force drops disastrously due

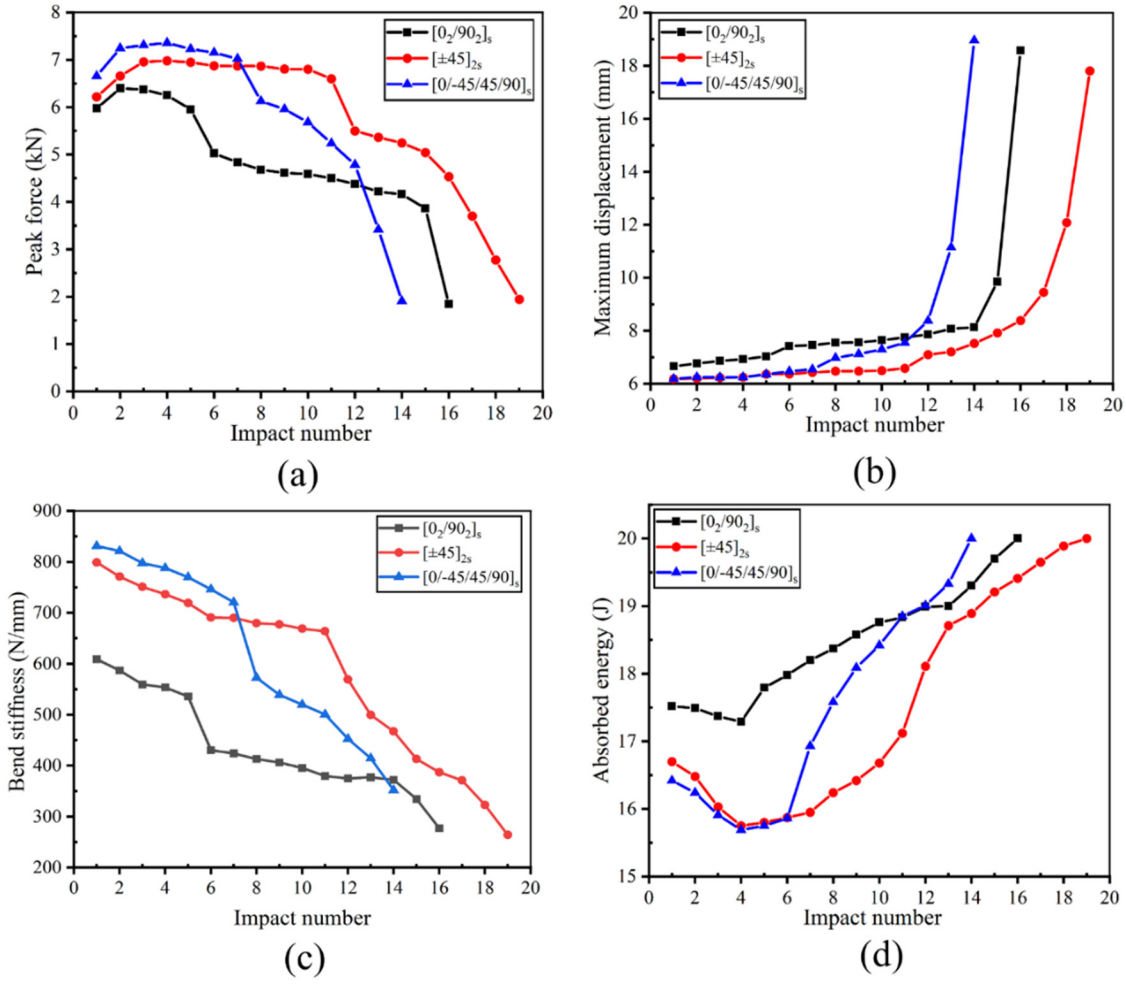

Figure 5: Changes in the impact characteristics with respect to the impact number: (a) peak force, (b) maximum displacement, (c) bending stiffness, and (d) absorbed energy.

to the loss of load bearing capacity of the specimens. On the whole, the peak force of the angle-ply $[\pm45°]_{2s}$ and quasi-isotropic $[0°/-45°/45°/90°]_s$ specimens is always higher than that of the sandwich-like $[0°_2/90°_2]_s$ specimen at the same impact number, which suggests that the former specimens possess a relatively higher load bearing capability. Hence, the impact resistance of the angle-ply and quasi-isotropic specimens is better than the sandwich-like specimen. Compared to the quasi-isotropic specimen, the peak force of the angle-ply specimen is little lower at initial few impact numbers caused by the lower impact bending stiffness, which is consistent with the results recorded in literature (39,40). However, the peak force of the quasi-isotropic specimen drops quickly after the impact number of the 7th corresponding occurrence of fiber breakage, which indicates the damage of this specimen induced by the fiber breakage develops much more fastly. This phenomenon is also caused by the large continuous delamination propagation illustrated below, which severely reduces the integrity of the specimen and degrades the load carrying capacity. As a consequence, the peak force of the quasi-isotropic specimen is lower than that of the angle-ply specimen in subsequent impacts, which demonstrates that the angle-ply laminate acquires better impact resistance under repeated low velocity impacts.

The variation in maximum central displacement with respect to the impact number is displayed in Figure 5(b). The maximum central displacement first increases very slowly before the 5th, 11th, and 7th impact for the specimens with the stacking sequences of $[0°_2/90°_2]_s$, $[\pm45°]_{2s}$, and $[0°/-45°/45°/90°]_s$, respectively. Then, it has an evident increase because of the sudden drop in impact bending stiffness arisen from fiber breakage. Subsequently, the maximum displacement gradually increases with the impact number rising before the penetration. At last, the maximum displacement has a dramatic increase due to the severe damage induced in the specimens. In addition, the rate of increase for the maximum displacement of the quasi-isotropic specimen is obviously larger than that of the sandwich-like and angle-ply specimens after the occurrence of fiber breakage, which indicates that the damage accumulation of this laminate is relatively faster. The gradually intensified fiber breakage and continuous delamination propagation interact with each other, resulting in the faster increase of the maximum central displacement of the quasi-isotropic specimen. On the whole, the maximum central displacement of the angle-ply specimen is the lowest among the three lay-up configurations at the same impact number, and the maximum displacement at the perforation event is also the lowest compared to the other two specimens. Meanwhile, the rate of increase for the maximum displacement of angle-ply specimen is relatively slow and stable throughout the repeated impacts. It thus can be concluded that the impact resistance of the angle-ply laminate is better subjected to repeated low velocity impacts.

The impact bending stiffness of the three laminated structures, obtained by the slope of the ascending phase in the force–displacement curves, is illustrated in Figure 5(c). As indicated in previous studies (17,32), the impact bending stiffness is closely associated with the damage evolution of the impacted laminates. It is evident that the bending stiffness first declines slowly for all prepared specimens, which is due to the gradual development of matrix cracking and delamination induced in the specimens. As revealed by Liao et al. (17), the reduction in impact bending stiffness of laminates is directly related to the propagation of delamination damage before the appearance of fiber breakage. Then, the bending stiffness shows a significant drop at the 6th, 12^{th}, and 8th impact, resulted from the impact-induced fiber breakage at the 5th, 11th, and 7th impact for the specimens with the ply orientations of $[0°_2/90°_2]_s$, $[\pm45°]_{2s}$, and $[0°/-45°/45°/90°]_s$, respectively. Finally, the bending stiffness continuously decreases as the impact-induced damage gradually intensifies at subsequent impacts until perforation.

In general, the bending stiffness of the angle-ply and quasi-isotropic specimens is always larger than that of the sandwich-like specimen at the same impact number, which indicates that the former two lay-up configurations can reserve the mechanical performance relatively better and less damage is induced in the laminates during the repeated impacts. It can also be seen that the bending stiffness of the quasi-isotropic specimen is a little higher than that of the angle-ply specimen before the appearance of fiber breakage, while it decreases sharply with the gradual accumulation of fiber breakage and is even lower than that of the angle-ply specimen in subsequent impacts. As shown in the following part, the continuous propagation of delamination damage also contributes to the degradation of the bending stiffness of the quasi-isotropic specimen. Therefore, the angle-ply laminate possesses the most superior impact resistance and damage tolerance among the three prepared laminates subjected to repeated impacts.

The change in absorbed energy relative to the impact number for the three kinds of specimens is shown in Figure 5(d). It is clear that the absorbed energy gradually decreases at first few impacts for all the prepared specimens. As analyzed above, the matrix cracking and delamination are the dominant damage modes during the initial few impacts. As indicated in previous studies (21,32), the first hit causes the major damage to the laminates when the damage induced in the central region of the laminate is primarily characterized by the matrix cracking and

delamination. Due to the compaction effect, the intact fibers support more impact loading relative to the damaged matrix, and the propagation of delamination is more or less restrained. Then, the absorbed energy gradually increases with the increase in the impact number, and an obvious increase in the absorbed energy is observed at the impact number of the appearance of fiber breakage. Finally, the absorbed energy almost reaches the initial impact energy at the 16th, 19th, and 14th impact for the first time, respectively. This means the occurrence of the perforation. In general, the absorbed energy of the sandwich-like specimen is larger than that of the angle-ply and quasi-isotropic specimens at the same impact number, which indicates that more damage is caused in the specimen and the impact resistance is weaker. The absorbed energy of quasi-isotropic specimen is lower than that of angle-ply specimen before the occurrence of fiber breakage at the same impact number, which demonstrates that the impact performance of quasi-isotropic laminate is more superior when the damage induced in laminates is dominated by the matrix cracking and delamination. Compared to the angle-ply specimen, the larger peak force and impact bending stiffness also prove the better impact resistance of the quasi-isotropic specimen for first few impacts. However, compared with the quasi-isotropic specimen, lower absorbed energy of the angle-ply specimen is clearly observed at each impact event in subsequent impacts, and the total energy dissipation is relatively higher owing to the more impact numbers until perforation. This indicates that less damage is induced at each strike in subsequent impact events and the damage tolerance is higher for the angle-ply laminate.

3.3 Damage morphology and damage evolution

The damage evolution of fiber-reinforced composite laminates under repeated low velocity impacts is extremely complex due to the damage accumulation effect. To a certain extent, the damage evolution of the impacted laminates can be revealed by the damage morphology recorded in each impact event. To acquire a clear observation on the damage morphology on both surfaces of the specimens, the central region with 100 mm × 60 mm in dimension is chosen as the damage is mainly induced surrounding the impact point.

The representative damage morphology on both surfaces of the three stacking specimens at the four stages is illustrated in Figure 6(a). A small quantity of matrix cracking on the front surface and delamination on the rear surface is observed for all the prepared specimens at stage I dominated by the matrix cracking damage. For the stage II of the delamination threshold, the matrix cracking on the front surface has a little propagation, while the delamination on the rear surface has an obvious development. After full expansion of matrix cracking and delamination beneath the impact position, the damage of fiber breakage is induced at stage III. It can be seen that a circular indention is left on the front surface, and large delamination with an evident hump is observed on the rear surface. The impactor has inserted into the specimens and abundant fiber breakage occurs at the central region of the specimens at stage IV of perforation. And the pit depths of 2.65, 2.37, and 2.22 mm are left in the composite laminates with the stacking sequences of $[0°_2/90°_2]_s$, $[\pm45°]_{2s}$, and $[0°/-45°/45°/90°]_s$, respectively. On the whole, the damage induced in the laminates becomes more severe with the increase in the impact number. By comparison, the matrix cracking in the front view propagates along the ply directions, namely, the 0°/90° direction for the specimen with the stacking sequence of $[0°_2/90°_2]_s$ and the +45°/−45° direction for the specimens with the lay-up sequence of $[\pm45°]_{2s}$, and the delamination in the rear view develops in an elliptical shape with the major axis along the stacking direction of the outermost layer, namely, the 0° direction for the sandwich-like specimen and the +45° direction for the angle-ply specimen. While, for the specimen with the ply orientation of $[0°/-45°/45°/90°]_s$, the matrix cracking on the front side propagates in all orientations, and the delamination on the back side extends approximately in a circular form. To make a more clear observation on the damage region caused in the composite laminates, the ultrasonic C-scan technology has been widely applied to determine the total projected delamination area. The delamination areas of the three stacking specimens with the selected central region of 100 mm × 60 mm in dimension at the four stages are also shown in Figure 6(b). The change in the delamination region and the delamination propagation are revealed more clearly by the C-scan images, which are consistent with the damage morphology discussed above. As reported in previous studies (41,42), the matrix cracking occurs parallel to the fibers first due to the debonding between the fiber and the matrix. Then, the delamination is triggered in the matrix-rich region when matrix cracking propagates to the interface between two adjacent plies with different orientations. And the delamination develops along the orientation of the bottom ply. Subsequently, after extreme development of matrix cracking and delamination, the fiber breakage is caused by the local high stress and the indentation influences of shear pressures. Finally, the laminate is embedded by the impactor when the damage of fiber breakage reaches a critical point, resulting in the perforation at the macroscopic level.

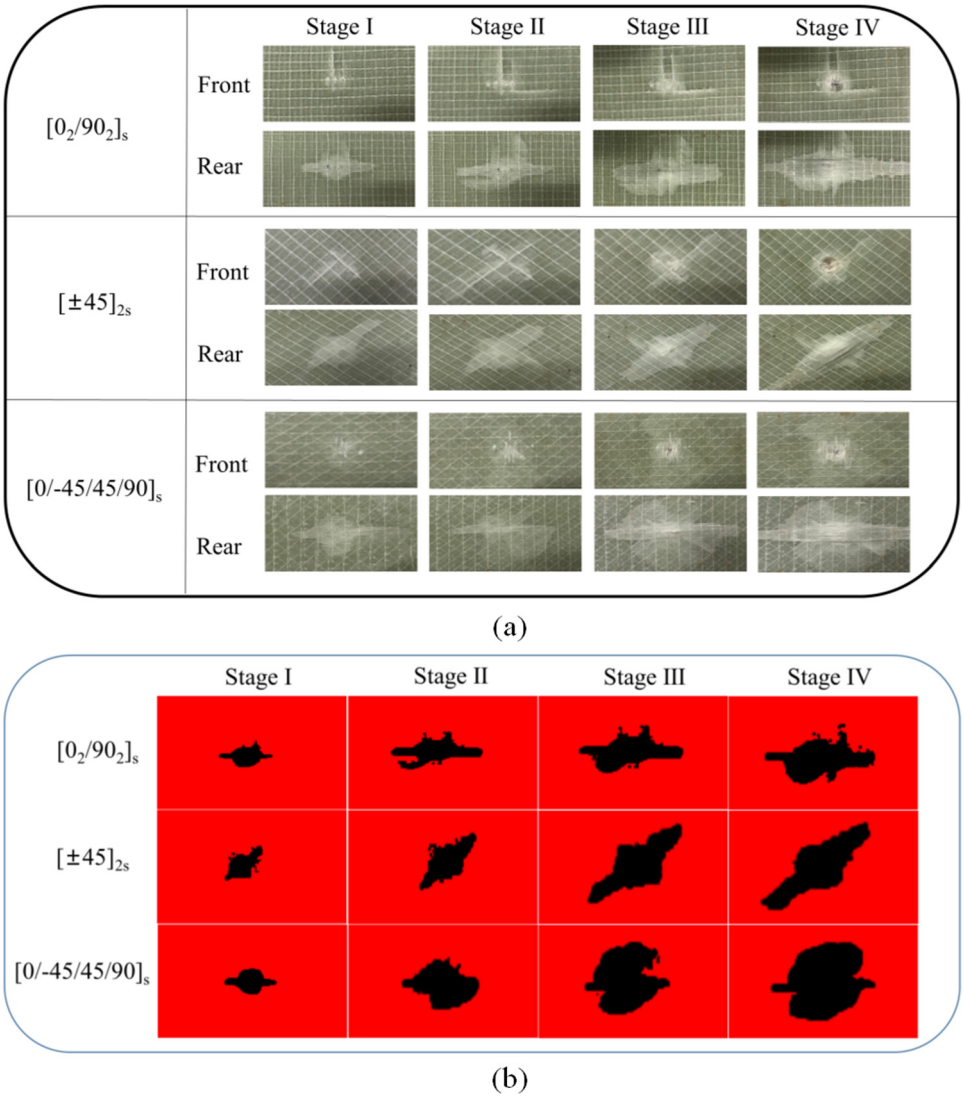

Figure 6: Damage caused in the three lay-up composite laminates: (a) Representative damage morphology observed on both surfaces (stage I represents the occurrence of large matrix cracking, stage II represents the delamination threshold, stage III denotes the appearance of fiber breakage, stage IV corresponds to the perforation) and (b) the ultrasonic C-scan results of the delamination projected area at the four stages.

Damage evolution of composite laminates is closely related to the development of damage induced, especially the interlaminar damage of delamination (21,38). To a certain extent, the damage evolution of composite laminates subjected to repeated impacts can be quantitated by the projected area of delamination. The projected delamination areas of the three kinds of specimens corresponding to the four stages and with respect to the impact number are displayed in Figure 7(a) and (b), respectively. The damage area is small for all the three stacking sequences at stage I owing to the delamination onset at the first impact. An evident increase is observed for the damage area at stage II due to the delamination propagation. Then, the damage area increases fast due to the rapid propagation of delamination before the appearance of fiber breakage at stage III. Finally, for the specimens with the stacking sequences of $[0°_2/90°_2]_s$ and $[\pm45°]_{2s}$, the damage area gradually increases until it roughly reaches a saturation value in subsequent impacts. This trend is consistent with the statement in previous works [43,44], i.e., the delamination area increases slowly after a certain number of impacts, and the delamination saturation is approximately reached when there is no new damage extended. While for the specimen with the lay-up sequence of $[0°/-45°/45°/90°]_s$, the damage area still keeps a fast increasing trend until the 11th impact, and then is close to a saturation value in subsequent few impacts. The projected damage areas are about 3,109.03, 3,069.77, and

6,075.44 mm^2 for the sandwich-like, angle-ply and quasi-isotropic specimens, respectively. It is evident that the saturation damage area of the quasi-isotropic specimen is about two times larger than that of the other two kinds of specimens. The fiber orientations of two adjacent plies are different except for the two middle plies in the quasi-isotropic specimen. Since the delamination occurs at the interface between two plies with different fiber orientations, the delamination still increases significantly after the appearance of fiber breakage, thus the delamination saturation is delayed and the projected damage area is larger. Hence, the damage tolerance is higher for the angle-ply specimen with less damage induced under repeated impacts.

To have a close understanding of the damage mechanism, the micro-damage morphology of the central impact region of the damaged specimens is illustrated in Figure 8, as detected by the SEM technique. The damage modes, including matrix cracking, fiber/matrix debonding, delamination, and fiber breakage, can be clearly distinguished for the three stacking specimens. The matrix cracking propagates along the fiber orientation due to the debonding between fiber and matrix, or extends through the thickness resulted from tension or shear. The delamination is easily found between two adjacent plies with different fiber orientations, as shown by SEM images. The fiber breakage occurs when the local high stress induced in the damaged region exceeds the load bearing capability of the fibers.

3.4 Damage accumulation evaluation

To assess the damage cumulative degree of the studied laminates subjected to repeated low velocity impacts from no damage to perforation, the damage accumulation parameters DI and DI-B are applied in this study, respectively. The damage variable DI was proposed by Belingardi et al. (35) to explore the damage accumulation in thick laminates from first impact to perforation. The parameter DI can not only reflect the trend of energy dissipation related to the impact number but also distinguish the penetration from the stable damage accumulation process. The variable DI is expressed as

$$\mathrm{DI} = \mathrm{DD}\frac{d_{\max}}{d_{\mathrm{p}}} \tag{1}$$

where $d_{\max}$ is the maximum displacement of the force–displacement curve in each impact event, and d_{p} is the critical displacement of the force–displacement curve at perforation. The parameter DD is defined as the absorbed energy fraction for each impact, namely,

$$\mathrm{DD} = \begin{cases} \dfrac{E_{\mathrm{a}}}{E_{\mathrm{i}}}, & \text{up to perforation} \\ \equiv 1, & \text{after perforation} \end{cases} \tag{2}$$

where E_{i} and E_{a} are the impact energy and absorbed energy, respectively. The calculated DI with respect to the impact number of the three stacking laminates under repeated impacts is displayed in Figure 9(a). Almost an invisible reduction in the DI is distinguished for the three studied laminates at first few impacts, caused by the decrease in DD. Subsequently, the variable DI first increases slowly and then rapidly with the rise in impact number for all the studied laminates, which is closely associated with the damage modes induced during the repeated impact process. Compared to the matrix cracking and delamination damage patterns dominated in the laminates at first few

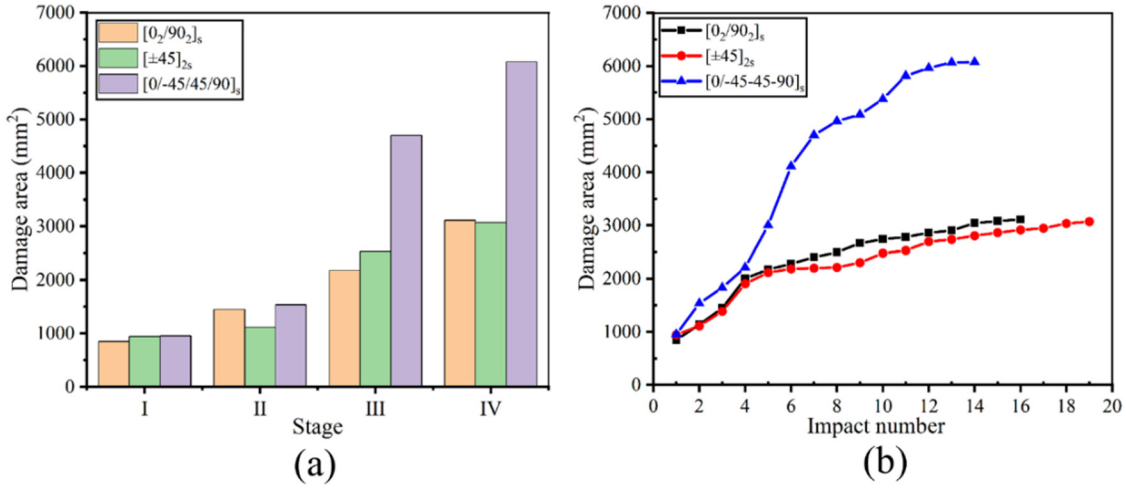

Figure 7: Projected delamination areas of the specimens: (a) damage area at the four stages and (b) damage area vs impact number curves.

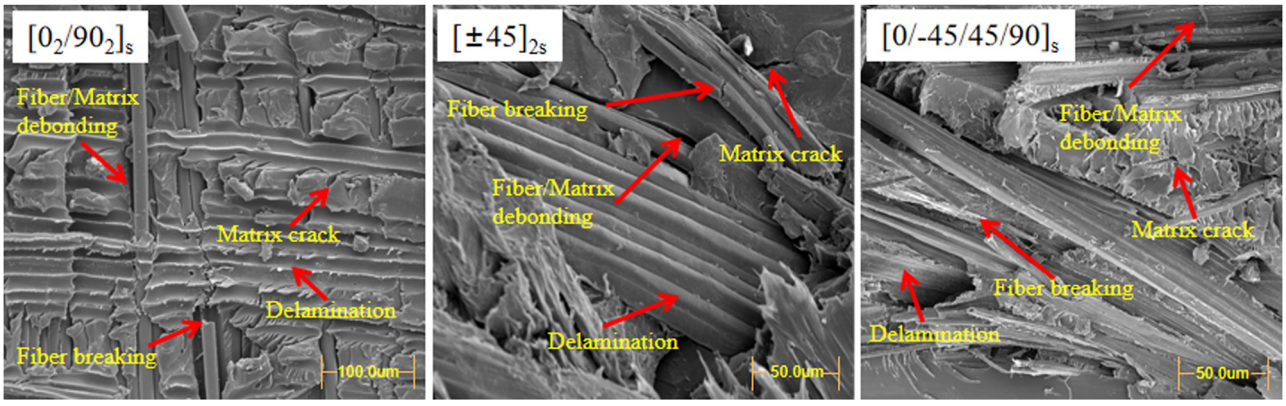

Figure 8: Micro-damage morphology of the three stacking sequences.

impacts, the damage of fiber breakage induced in subsequent impacts causes large degradation of the mechanical performance, leading to the damage accumulation more rapidly. In general, the variable DI of the laminate with the ply orientation of $[0°_2/90°_2]_s$ is larger than that of the other two laminates, which indicates that the impact resistance of the sandwich-like laminate is weaker with severe damage accumulated in the laminate during repeated impacts. Moreover, the variable DI of the laminate with the stacking sequence of $[0°/-45°/45°/90°]_s$ is smaller than that of the laminate with the lay-up sequence of $[\pm45°]_{2s}$ before the 7th impact, which demonstrates that the impact resistance of the quasi-isotropic laminate is better at initial several impacts. While, the variable DI of the quasi-isotropic laminate increases rapidly in subsequent impacts, even larger than that of the angle-ply laminate. This phenomenon proves that the impact performance is better for the angle-ply laminate in subsequent impacts. The damage variable DI can reflect the tendency of the damage accumulation of the three studied laminates, and identify the occurrence of perforation. However, variable DI fails to meet the logic of damage index for characterizing the damage accumulation monotonically increasing from zero to one.

The damage variable DI-B developed by Liao et al. (17) is employed to characterize the damage accumulation more generally. Based on the impact bending stiffness reduction rate R_s and normalized maximum displacement, the variable DI-B is defined as follows:

$$\text{DI-B} = R_s \frac{d_{\max}}{d_p} \tag{3}$$

where R_s can be calculated as follows:

$$R_s = \frac{k_0 - k_i}{k_0 - k_f} \tag{4}$$

where k_0 stands for the initial impact bending stiffness at first impact, k_f represents the bending stiffness at

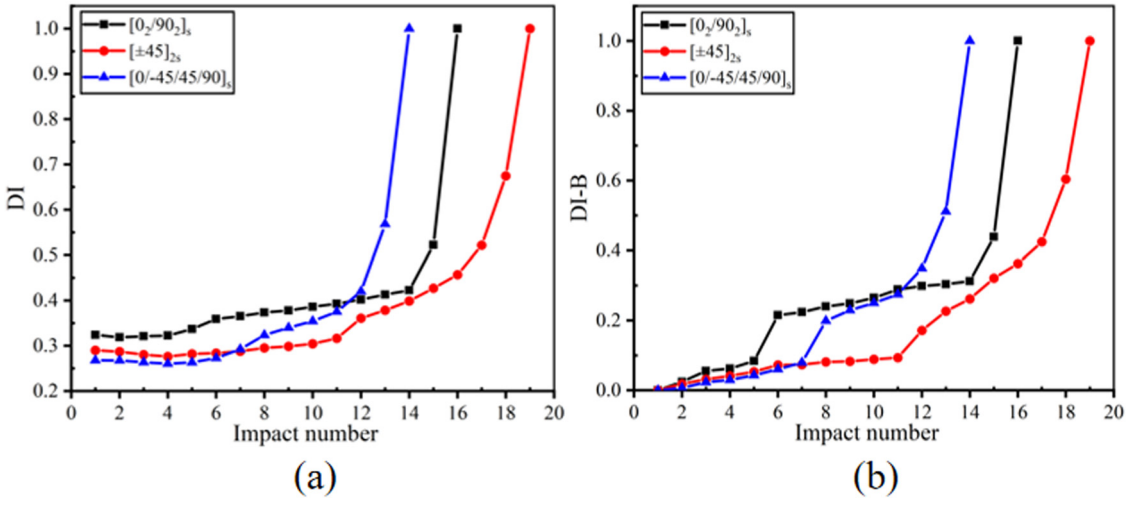

Figure 9: Damage accumulation characterized by different damage variables: (a) DI and (b) DI-B.

perforation, and k_i is the bending stiffness at the ith impact. The tendency of the damage variable DI-B with respect to the impact number is shown in Figure 9(b). It is easily observed that the DI-B monotonically increases from zero to one attributed to the bending stiffness reduction rate monotonically increasing from zero to one. The occurrence of matrix cracking and delamination, damage accumulation phase dominated by matrix cracking and delamination, appearance of fiber breakage, damage accumulation phase dominated by fiber breakage, and perforation are distinguished for the studied laminates subjected to repeated impacts. Compared to the other two composite laminates, it is evident that more impact numbers are required to reach the value one of the DI-B index for the angle-ply laminate, which indicates the damage tolerance of the angle-ply laminate is higher, i.e., the angle-ply laminate can withstand more repeated impacts and thus dissipate more impact energy. Furthermore, the damage accumulation of the angle-ply laminate is the slowest among the three studied composite laminates on the whole, which demonstrates that the impact resistance of this laminate is the best. The slower the increase in damage accumulation, the lesser the damage caused at each impact event, and hence better the impact resistance. Compared with the sandwich-like laminate, the damage propagation through the thickness can be limited or stopped by alternating fiber orientation in adjacent plies for the angle-ply laminate, thus less damage is induced at each impact event. Compared to the synergistic action of the severe fiber breakage development and continuous delamination extension in the quasi-isotropic laminate after the appearance of fiber breakage, the damage accumulation in the angle-ply laminate is mainly induced by the stable fiber breakage propagation due to the delamination saturation. As a consequence, the damage accumulation of the angle-ply laminate is relatively slower and stabler. Therefore, the angle-ply laminate possesses higher impact resistance and damage tolerance than the quasi-isotropic laminate.

4 Conclusion

The dynamic response and damage accumulation of glass fiber-reinforced composite laminates subjected to repeated low velocity impacts were investigated in this study. The purpose of this work was to analyze the influence of lay-up sequences on the impact resistance of this composite under repeated impacts. The composite laminates with three different lay-up sequences, including sandwich-like, angle-ply, and quasi-isotropic configurations, were impacted at 20 J in each impact until perforation. The following conclusions can be drawn:

1. The force–time/maximum displacement curves show that the matrix cracking, delamination initiation, fiber breakage, and perforation are the four typical impact characteristics describing the damage evolution of repeated impacts. Compared with a roughly circular shape for the quasi-isotropic laminate, the delamination of the sandwich-like and angle-ply laminates primarily develops in an elliptical shape with the major axis along the stacking direction of the outermost layer during repeated impacts.
2. The impact resistance of the sandwich-like laminate is the weakest among the three stacking structures with the lowest peak force, the highest maximum displacement, and the smallest bending stiffness.
3. Compared with the angle-ply laminate, the impact performance of the quasi-isotropic is better with larger bending stiffness before the appearance of fiber breakage. On the contrary, the angle-ply laminate possesses higher impact resistance and damage tolerance with relatively slower damage accumulation at subsequent impacts.
4. Compared with the damage variable DI, the DI-B meets the logic of damage index monotonically increasing from zero to one, and can characterize the damage accumulation and perforation simultaneously for the current studied composite laminates.

Funding information: This work was supported by the National Natural Science Foundation of China (12162013), the Natural Science Foundation of Jiangxi Province, China (20212BAB214013).

Author contributions: Zhaogang Yu: writing – original draft, conducting the experiment, and characterization; Kun Liu: writing – review and editing; Zhen Tao: writing – review and editing; Jangtao Zhang: writing – review and editing; Hao Li: writing – review and editing and project administration.

Conflict of interest: The authors state no conflict of interest.

Data availability statement: The data that support the findings of this study are available from the corresponding author upon reasonable request.

References

(1) Rani M, Choudhary P, Krishnan V, Zafar S. A review on recycling and reuse methods for carbon fiber/glass fiber composites waste from wind turbine blades. Compos Part B-Eng. 2021;215:108768.

(2) Rubino F, Nisticò A, Tucci F, Carlone P. Marine application of fiber reinforced composites: A review. J Mar Sci Eng. 2020;8(1):26.
(3) Li J, Durandet Y, Huang X, Sun G, Ruan D. Additively manufactured fiber-reinforced composites: A review of mechanical behavior and opportunities. J Mater Sci Technol. 2022;119:219–44.
(4) Giridharan R. Preparation and property evaluation of Glass/Ramie fibers reinforced epoxy hybrid composites. Compos Part B-Eng. 2019;167:342–5.
(5) Gemi DS, Şahin ÖS, Gemi L. Experimental investigation of the effect of diameter upon low velocity impact response of glass fiber reinforced composite pipes. Compos Struct. 2021;275:114428.
(6) Boukar A, Corn S, Slangen PR, Ienny P. Finite element modelling of low velocity impact test applied to biaxial glass fiber reinforced laminate composites. Int J Impact Eng. 2022;165:104218.
(7) Chen D, Luo Q, Meng M, Li Q, Sun G. Low velocity impact behavior of interlayer hybrid composite laminates with carbon/glass/basalt fibres. Compos Part B-Eng. 2019;176:107191.
(8) Daelemans L, Cohades A, Meireman T, Beckx J, Spronk S, Kersemans M, et al. Electrospun nanofibrous interleaves for improved low velocity impact resistance of glass fibre reinforced composite laminates. Mater Design. 2018;141:170–84.
(9) Barouni AK, Dhakal HN. Damage investigation and assessment due to low-velocity impact on flax/glass hybrid composite plates. Compos Struct. 2019;226:111224.
(10) Ozdemir O, Oztoprak N, Kandas H. Single and repeated impact behaviors of bio-sandwich structures consisting of thermoplastic face sheets and different balsa core thicknesses. Compos Part B-Eng. 2018;149:49–57.
(11) Macdonald H, Nash D, Stack MM. Repeated impact of simulated hail ice on glass fibre composite materials. Wear. 2019;432:102926.
(12) Arikan V, Sayman O. Comparative study on repeated impact response of E-glass fiber reinforced polypropylene & epoxy matrix composites. Compos Part B-Eng. 2015;83:1–6.
(13) Li L, Sun L, Wang T, Kang N, Cao W. Repeated low-velocity impact response and damage mechanism of glass fiber aluminium laminates. Aerosp Sci Technol. 2019;84:995–1010.
(14) Balcı O, Çoban O, Bora MÖ, Akagündüz E, Yalçin EB. Experimental investigation of single and repeated impacts for repaired honeycomb sandwich structures. Mater Sci Eng A-Struct. 2017;682:23–30.
(15) Kashani MH, Sadighi M, Lalehpour A, Alderliesten RC. The effect of impact energy division over repeated low-velocity impact on fiber metal laminates. J Compos Mater. 2015;49(6):635–46.
(16) Dogan A. Single and repeated low-velocity impact response of E-glass fiber-reinforced epoxy and polypropylene composites for different impactor shapes. J Thermoplast Compos. 2022;35(3):320–36.
(17) Liao B, Zhou J, Li Y, Wang P, Xi L, Gao R, et al. Damage accumulation mechanism of composite laminates subjected to repeated low velocity impacts. Int J Mech Sci. 2020;182:105783.
(18) Atas C, Dogan A. An experimental investigation on the repeated impact response of glass/epoxy composites subjected to thermal ageing. Compos Part B-Eng. 2015;75:127–34.
(19) Zhu L, Guo K, Li Y, Yu TX, Zhou Q. Experimental study on the dynamic behaviour of aluminium foam sandwich plates under single and repeated impacts at low temperature. Int J Impact Eng. 2018;114:123–32.
(20) Coelho SRM, Reis PNB, Ferreira JAM, Pereira AM. Effects of external patch configuration on repaired composite laminates subjected to multi-impacts. Compos Struct. 2017;168:259–65.
(21) Sun Z, Li C, Tie Y. Experimental and numerical investigations on damage accumulation and energy dissipation of patch-repaired CFRP laminates under repeated impacts. Mater Design. 2021;202:109540.
(22) Sadighi M, Tooski MY, Alderliesten RC. An experimental study on the low velocity impact resistance of fibre metal laminates under successive impacts with reduced energies. Aerosp Sci Technol. 2017;67:54–61.
(23) Tian S, Zhou Z. New criteria for simulating failure under multiple impacts of the same total energy on glass fiber reinforced aluminum alloy laminates. Mater Design. 2016;102:142–50.
(24) Akatay A, Bora MÖ, Çoban O, Fidan S, Tuna V. The influence of low velocity repeated impacts on residual compressive properties of honeycomb sandwich structures. Compos Struct. 2015;125:425–33.
(25) Guo K, Zhu L, Li Y, Yu TX, Shenoi A, Zhou Q. Experimental investigation on the dynamic behaviour of aluminum foam sandwich plate under repeated impacts. Compos Struct. 2018;200:298–305.
(26) Garzon-Hernandez S, Garcia-Gonzalez D, Arias A. Multi-impact mechanical behaviour of short fibre reinforced composites. Compos Struct. 2018;202:241–52.
(27) Saleh MN, El-Dessouky HM, Saeedifar M, De Freitas ST, Scaife RJ, Zarouchas D. Compression after multiple low velocity impacts of NCF, 2D and 3D woven composites. Compos Part A-Appl Sci Manuf. 2019;125:105576.
(28) Sevkat E, Liaw B, Delale F, Raju BB. Effect of repeated impacts on the response of plain-woven hybrid composites. Compos Part B-Eng. 2010;41(5):403–13.
(29) David-West OS, Nash DH, Banks WM. An experimental study of damage accumulation in balanced CFRP laminates due to repeated impact. Compos Struct. 2008;83(3):247–58.
(30) Atas C, Icten BM, Küçük M. Thickness effect on repeated impact response of woven fabric composite plates. Compos Part B-Eng. 2013;49:80–5.
(31) Paolino DS, Cavatorta MP, Belingardi G. Effect of thickness on the damage tolerance of glass/epoxy laminates subject to repeated impacts. P I Mech Eng C-J Mech Eng Sci. 2018;232(8):1363–73.
(32) Rezasefat M, Gonzalez-Jimenez A, Giglio M, Manes A. Numerical study on the dynamic progressive failure due to low-velocity repeated impacts in thin CFRP laminated composite plates. Thin Wall Struct. 2021;167:108220.
(33) González EV, Maimí P, Camanho PP, Lopes CS, Blanco N. Effects of ply clustering in laminated composite plates under low-velocity impact loading. Compos Sci Technol. 2011;71(6):805–17.
(34) Papa I, Formisano A, Lopresto V, Langella A. Low velocity impact behaviour of reinforced plastic laminates: Indentation and penetration laws validated for different fibres and matrices. Compos Part B-Eng. 2019;164:61–6.
(35) Belingardi G, Cavatorta MP, Paolino DS. On the rate of growth and extent of the steady damage accumulation phase in repeated impact tests. Compos Sci Technol. 2009;69(11–12):1693–8.
(36) Fragassa C, Pavlovic A, Santulli C. Mechanical and impact characterisation of flax and basalt fibre vinyl ester composites and their hybrids. Compos Part B-Eng. 2018;137:247–59.
(37) Quaresimin M, Ricotta M, Martello L, Mian S. Energy absorption in composite laminates under impact loading. Compos Part B-Eng. 2013;44(1):133–40.
(38) Wang C, Chen Z, Silberschmidt VV, Roy A. Damage accumulation in braided textiles-reinforced composites under repeated impacts: Experimental and numerical studies. Compos Struct. 2018;204:256–67.

(39) Caminero MA, García-Moreno I, Rodríguez GP. Damage resistance of carbon fibre reinforced epoxy laminates subjected to low velocity impact: Effects of laminate thickness and ply-stacking sequence. Polym Test. 2017;63:530–41.
(40) Lebaupin Y, Hoang TQT, Chauvin M, Touchard F. Influence of the stacking sequence on the low-energy impact resistance of flax/PA11 composite. J Compos Mater. 2019;53(22):3187–98.
(41) Lopes CS, Seresta O, Coquet Y, Gürdal Z, Camanho PP, Thuis B. Low-velocity impact damage on dispersed stacking sequence laminates. Part I: Experiments. Compos Sci Technol. 2009;69(7–8):926–36.
(42) Sebaey TA, González EV, Lopes CS, Blanco N, Costa J. Damage resistance and damage tolerance of dispersed CFRP laminates: Effect of ply clustering. Compos Struct. 2013;106:96–103.
(43) Azouaoui K, Rechak S, Azari Z, Benmedakhene S, Laksimi A, Pluvinage G. Modelling of damage and failure of glass/epoxy composite plates subject to impact fatigue. Int J fatigue. 2001;23(10):877–85.
(44) Tooski MY, Alderliesten RC, Ghajar R, Khalili SMR. Experimental investigation on distance effects in repeated low velocity impact on fiber–metal laminates. Compos Struct. 2013;99:31–40.